Optical recoil of asymmetric nano-optical antenna

Jung-Hwan Song,[1] Jonghwa Shin,[1,*] Hee-Jin Lim,[1] and Yong-Hee Lee[1,2]

[1]*Department of Physics, Korea Advanced Institute of Science and Technology, Daejeon 305-701, Korea*
[2]*Department of Physics and Department of Nanoscience and Technology (WCU), Korea Advanced Institute of Science and Technology, Daejeon 305-701, Korea*
**jshin@jshin.info*

Abstract: We propose nano-optical antennas with asymmetric radiation patterns as light-driven mechanical recoil force generators. Directional antennas are found to generate recoil force efficiently when driven in the spectral proximity of their resonances. It is also shown that the recoil force is equivalent to the Poynting vector integrated over a closed sphere containing the antenna structures.

OCIS codes: (240.6680) Surface plasmons; (260.3910) Metal optics; (350.4855) Optical tweezers or optical manipulation; (350.5610) Radiation.

References and links

1. A. Ashkin and J. M. Dziedzic, "Optical levitation by radiation pressure," Appl. Phys. Lett. **19**(8), 283–335 (1971).
2. S. Chu, J. E. Bjorkholm, A. Ashkin, and A. Cable, "Experimental observation of optically trapped atoms," Phys. Rev. Lett. **57**(3), 314–317 (1986).
3. S. Mandal, X. Serey, and D. Erickson, "Nanomanipulation using silicon photonic crystal resonators," Nano Lett. **10**(1), 99–104 (2010).
4. S. Lin, E. Schonbrun, and K. Crozier, "Optical manipulation with planar silicon microring resonators," Nano Lett. **10**(7), 2408–2411 (2010).
5. M. Liu, T. Zentgraf, Y. Liu, G. Bartal, and X. Zhang, "Light-driven nanoscale plasmonic motors," Nat. Nanotechnol. **5**(8), 570–573 (2010).
6. L. Novotny and B. Hecht, *Principles of Nano-Optics* (Cambridge University Press, 2007).
7. A. Taflove and S. C. Hagness, *Computational Electrodynamics: The Finite-Difference Time-Domain Method* (Artech House, 2005).
8. S. Uda, "Wireless beam of short electric waves," J. IEE (Japan) **452**, 273–282 (1926).
9. H. Yagi, "Beam transmission of ultra short waves," in *Proceedings of IRE Conference*, pp. 715–741.
10. A. W. Rudge, "Offset-parabolic-reflector antennas: a review," in *Proceedings of IEEE Conference* (1978), pp. 1592–1618.
11. T. Pakizeh and M. Käll, "Unidirectional ultracompact optical nanoantennas," Nano Lett. **9**(6), 2343–2349 (2009).
12. T. Pakizeh, M. S. Abrishamian, N. Granpayeh, A. Dmitriev, and M. Käll, "Magnetic-field enhancement in gold nanosandwiches," Opt. Express **14**(18), 8240–8246 (2006).
13. T. H. Taminiau, F. D. Stefani, and N. F. van Hulst, "Enhanced directional excitation and emission of single emitters by a nano-optical Yagi-Uda antenna," Opt. Express **16**(14), 10858–6 (2008).
14. J. D. Joannopoulos, R. D. Meade, and J. N. Winn, *Photonic Crystals* (Princeton University Press, 1995), Chap. 2.
15. E. Prodan, C. Radloff, N. J. Halas, and P. Nordlander, "A hybridization model for the plasmon response of complex nanostructures," Science **302**(5644), 419–422 (2003).
16. C. A. Balanis, *Antenna Theory* (John Wiley & Sons, 2005).
17. T. Kosako, Y. Kadoya, and H. F. Hofmann, "Directional control of light by a nano-optical Yagi-Uda antenna," Nat. Photonics **4**(5), 312–315 (2010).

1. Introduction

The curiosity about the mechanical effect of light goes back as early as the year of 1619 when Johannes Keppler suggested that light is responsible for the deflection of the tails of comets. Through the work of Maxwell's electromagnetic theory in 1873 it was shown that the radiation field carries linear momentum.

There are two well-known kinds of optical force. One is the scattering force that an object feels when it scatters incident light wave. Ashkin et al. utilized the scattering force to levitate dielectric particles [1]. The other is the gradient force that is observed when a polarizable object is placed in inhomogeneous electromagnetic fields. The gradient force pushes the

#148562 - $15.00 USD Received 1 Jun 2011; revised 23 Jun 2011; accepted 8 Jul 2011; published 19 Jul 2011

object in the direction of high or low field intensity region, depending on the dielectric constant of the object relative to that of the surrounding medium. Chu and associates demonstrated a novel particle manipulation technique, optical trapping, using the gradient force [2].

Recently, various non-invasive optical manipulation techniques have been developed for precise control of small particles. Typical examples include near-field trapping of dielectric beads using photonic crystal resonators [3], orbiting beads on a ring-shaped resonator [4], revolving dielectric disk which contains plasmonic structures [5].

In this paper, we investigate another kind of optical force, "recoil force," that an electromagnetic radiator experiences when it emits photons. It is shown that antennas with asymmetric radiation patterns receive net recoil force. In section 2 we show that the optical recoil force computed by Maxwell's stress tensor method is equivalent to that obtained by Poynting vector integration method. In section 3 we investigate three kinds of dipolar oscillators and show that an asymmetric radiation pattern results in non-zero recoil force. Here, we define a quantity, "force conversion efficiency," to evaluate the recoil force an electromagnetic radiator can acquire when it emits unit radiation power. In section 4 we suggest directional nano-optical antenna as an efficient force generator. In section 5 we summarize the results.

2. Recoil force

The optical far-field of a radiator represents the angular distribution of the emitted photon momentum vector. In other words, the total momentum transferred from a radiant source can be obtained by Poynting vector integration of corresponding far fields. In this section, we show the optical force obtained by this intuitive vector summation method is equivalent to that computed by the Maxwell's stress tensor method.

In order to calculate the force acting on a system placed in electromagnetic fields, we employ Maxwell's stress tensor,

$$\vec{\vec{T}} = \varepsilon_0 \vec{E} \otimes \vec{E} + \mu_0 \vec{H} \otimes \vec{H} - \frac{1}{2}(\varepsilon_0 |\vec{E}|^2 + \mu_0 |\vec{H}|^2)\vec{\vec{I}}, \tag{1}$$

in which ε_0 and μ_0 are the permittivity and the permeability in vacuum, respectively. $\otimes$ is the symbol expressing the dyadic product by which two vectors are transformed into a second order tensor. The time-averaged mechanical force on a system can be obtained by integrating Maxwell's stress tensor over the surface enclosing the system [6].

$$\left\langle \vec{F}(\vec{r},t) \right\rangle = \int_{\partial V} \left\langle \vec{\vec{T}}(\vec{r},t) \right\rangle \cdot \hat{n}(\vec{r}) da. \tag{2}$$

Fields in the brackets represent time-averaged values, ∂V is the enclosing surface over the system, $\hat{n}$ is the unit normal vector on the surface.

Imposing additional conditions, we can transform the Maxwell's stress tensor into a more intuitive form. The first condition is the orthogonality of electric field and magnetic field:

$$\hat{e}(\vec{r},t) \perp \hat{h}(\vec{r},t), \tag{3a}$$

$$\vec{E} = E(\vec{r},t)\hat{e}(\vec{r},t), \tag{3b}$$

$$\vec{H} = H(\vec{r},t)\hat{h}(\vec{r},t), \tag{3c}$$

$$\hat{s}(\hat{r},t) = \hat{e}(\vec{r},t) \times \hat{h}(\vec{r},t), \tag{3d}$$

where E and H are field amplitudes. $\hat{e}$ and $\hat{h}$ are the unit vectors of electric and magnetic field, respectively. Since the Poynting vector direction, $\hat{s}$, is the outer product of $\hat{e}$ and $\hat{h}$, $\hat{e}$,

#148562 - $15.00 USD Received 1 Jun 2011; revised 23 Jun 2011; accepted 8 Jul 2011; published 19 Jul 2011

$\hat{h}$, and $\hat{s}$ form a basis for a right-handed Cartesian coordinate system. Substituting the expressions in Eq. (3) into Eq. (1), the Maxwell's stress tensor becomes a simple diagonal matrix in this new local coordinate.

$$\ddot{T} = \begin{bmatrix} \frac{\varepsilon_0 E^2}{2} - \frac{\mu_0 H^2}{2} & 0 & 0 \\ 0 & -\frac{\varepsilon_0 E^2}{2} + \frac{\mu_0 H^2}{2} & 0 \\ 0 & 0 & -\frac{\varepsilon_0 E^2}{2} - \frac{\mu_0 H^2}{2} \end{bmatrix}. \quad (4)$$

Deriving Eq. (4), we used the following identifications of three dyadic products of the unit vectors.

$$\hat{e}\otimes\hat{e} = \begin{bmatrix} 1 & 0 & 0 \\ 0 & 0 & 0 \\ 0 & 0 & 0 \end{bmatrix}, \ \hat{h}\otimes\hat{h} = \begin{bmatrix} 0 & 0 & 0 \\ 0 & 1 & 0 \\ 0 & 0 & 0 \end{bmatrix}, \ \hat{s}\otimes\hat{s} = \begin{bmatrix} 0 & 0 & 0 \\ 0 & 0 & 0 \\ 0 & 0 & 1 \end{bmatrix}.$$

The second condition is the equality of the electric energy density ($\varepsilon_0 E^2/2$) and the magnetic energy density ($\mu_0 H^2/2$) which makes the Maxwell's stress tensor even simpler.

$$\ddot{T} = \begin{bmatrix} 0 & 0 & 0 \\ 0 & 0 & 0 \\ 0 & 0 & -\frac{\varepsilon_0 E^2 + \mu_0 H^2}{2} \end{bmatrix} = -\frac{|\vec{E}\times\vec{H}|\,\hat{s}\otimes\hat{s}}{c} = -\frac{S}{c}\hat{s}\otimes\hat{s}. \quad (5)$$

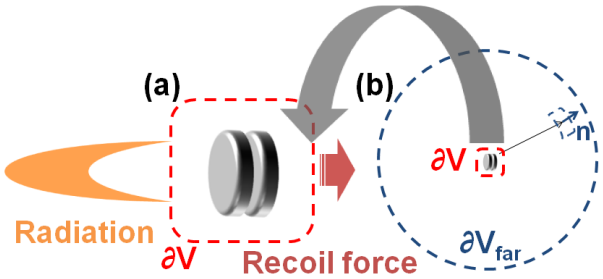

Fig. 1. Calculations of the recoil force on a radiator (a) by integrating Maxwell's stress tensor over an enclosing surface "∂V" and (b) by vector summation of Poynting vectors over the far-field sphere "∂V_{far}".

Now, we calculate the mechanical force on a radiator by integrating the Maxwell's stress tensor over the surface ∂V as depicted in Fig. 1(a). The time-averaged force on the radiator is calculated using Eq. (2). If we change the surface from ∂V to the far-field sphere [∂V_{far} in Fig. 1(b)], the above conditions are satisfied. Then we can substitute $\ddot{T}$ in Eq. (2) with the right hand side of Eq. (5) to obtain the following form.

$$\left\langle \vec{F}(\vec{r},t)\right\rangle = \int_{\partial V_{far}} \left\langle -\frac{S}{c}\hat{s}\otimes\hat{s}\right\rangle \cdot \hat{n}da = -\int_{\partial V_{far}} \left\langle \frac{\vec{S}}{c}\right\rangle da. \quad (6)$$

#148562 - $15.00 USD Received 1 Jun 2011; revised 23 Jun 2011; accepted 8 Jul 2011; published 19 Jul 2011

The last equality in Eq. (6) is derived using the fact that $\hat{n}$ equals $\hat{s}$ at the far-field sphere. The Eq. (6) corresponds to physical intuition that a radiating source feels the recoil force toward the opposite direction of the radiation pressure.

3. Force conversion efficiency

In order to quantify a radiator's ability to generate the recoil force, we introduce *Force conversion efficiency*, η_i, which is defined as the i-component (i = x, y, z) of mechanical force that the radiator experiences, normalized to the total radiated power, in units of 1/c. In other words, it is the ratio of the recoil force a radiator actually feels to the theoretical recoil force that results when the same amount of power is radiated toward a single direction.

$$\eta_i = \frac{\int_{\partial V_{far}} \left\langle \vec{S} \cdot \hat{i} \right\rangle da}{\int_{\partial V_{far}} \left\langle \vec{S} \cdot \hat{n} \right\rangle da}, \tag{7a}$$

$$\left\langle \vec{F} \right\rangle = -\frac{1}{c} \int_{\partial V_{far}} \left\langle \vec{S} \right\rangle da = -\frac{1}{c} (\eta_x \hat{x} + \eta_y \hat{y} + \eta_z \hat{z}) \int_{\partial V_{far}} \left\langle \vec{S} \cdot \hat{n} \right\rangle da. \tag{7b}$$

The force conversion efficiency is therefore a dimensionless quantity and approaches 1 when the most of energy is radiated toward a particular direction. On the contrary, it vanishes when the radiation is symmetric. Thus, the asymmetry in the radiation pattern is the indication of non-zero recoil force.

Let's consider the case of a simple monochromatic electric dipole oscillator. Firstly, we obtain the electric- and the magnetic-field data on the surface enclosing the oscillator using three-dimensional finite difference time domain (3D-FDTD) method. From this data, we can calculate the force directly by integrating the Maxwell's stress tensor. However, we also want to examine the radiation pattern to get physical intuition. So, we calculate the Poynting vector over the far-field sphere using Green's function method [7]. The recoil force on the oscillator is the vector summation of the Poynting vectors. Dividing the recoil force by the total radiation power one can obtain the force conversion efficiency.

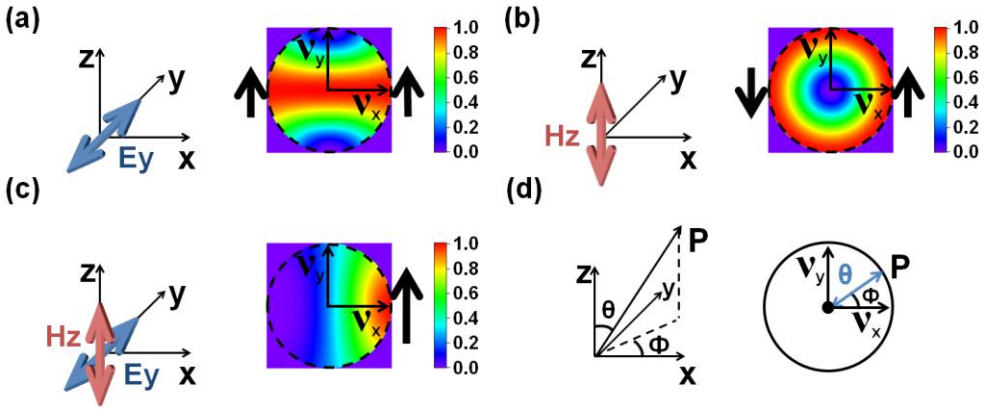

Fig. 2. The far-field radiation patterns of (a) y-directed electric dipole oscillator and (b) z-directed magnetic dipole oscillator and (c) the combination of y-directed electric dipole and z-directed magnetic dipole oscillators. The dashed black circles indicate the equator ($\theta = \pi/2$). (d) The coordinate for the far-field radiation pattern plots. v_x and v_y are directional cosines in x and y directions, respectively. The radius from the center indicates the polar angle ($0 \le \theta \le \pi/2$) between the observation point P and the z-axis. The angle (ϕ) is the azimuthal angle of the observation point P. The black arrows at the sides of far-field pattern indicate the electric field direction.

#148562 - $15.00 USD Received 1 Jun 2011; revised 23 Jun 2011; accepted 8 Jul 2011; published 19 Jul 2011

The first example is a y-directed electric dipole oscillator. It has the well-known toroidal radiation pattern shown in Fig. 2(a) and the axis of the toroid is the y-axis. Since the radiation is symmetric the force conversion efficiency is 0. We also note that, on the y = 0 plane, the electric field vector is identical in amplitude and phase at a constant distance from the origin.

The second example is a z-directed magnetic dipole oscillator [Fig. 2(b)]. The radiation pattern is the same as that of the electric dipole oscillator except that the toroidal axis is the z-axis. The force conversion efficiency is 0, likewise. The electric field vector on the y = 0 plane, however, has odd vector symmetry with respect to the z-axis, and the electric fields at (x, 0, 0) and (-x, 0, 0) are pointing in opposite directions ($\pm\hat{y}$).

The situation changes noticeably if we consider the combination of the y-directed electric and the z-directed magnetic dipoles [Fig. 2(c)]. If the two dipoles are oscillating in phase, the electric fields from the electric dipole and the magnetic dipole interfere constructively in the + x direction. On the other hand, they interfere destructively in the –x direction and cancel out each other such that the radiation becomes asymmetric along the x-axis [Fig. 2(c)]. We investigate this radiator by analytic methods and the far-field radiation pattern is obtained in a closed form.

$$S(\theta,\phi)=\frac{3}{8\pi}(\sin\theta\cos\phi+1)^2, \tag{8}$$

where the normalized intensity S is described as a function of the spherical coordinate angles, θ and ϕ, such that it gives unit radiation power when integrated over the total solid angle. The analytic solution is in accord with that predicted by the numerical methods [Fig. 2(c)]. Because of the asymmetric radiation in the x direction, there is non-zero recoil force in that direction. By analytic integration, the force conversion efficiency of 0.5 is obtained.

4. Asymmetric nano-optical antenna

There are various structures which radiate asymmetrically. Antenna structures such as Yagi-Uda antenna [8,9] and parabolic reflectors [10] are examples. Here, we investigate two kinds of directional nano-optical antenna. The examples are coupled nano-disk structure [Fig. 3(a)] and optical Yagi-Uda antenna [Fig. 3(d)] [11–13].

#148562 - $15.00 USD Received 1 Jun 2011; revised 23 Jun 2011; accepted 8 Jul 2011; published 19 Jul 2011

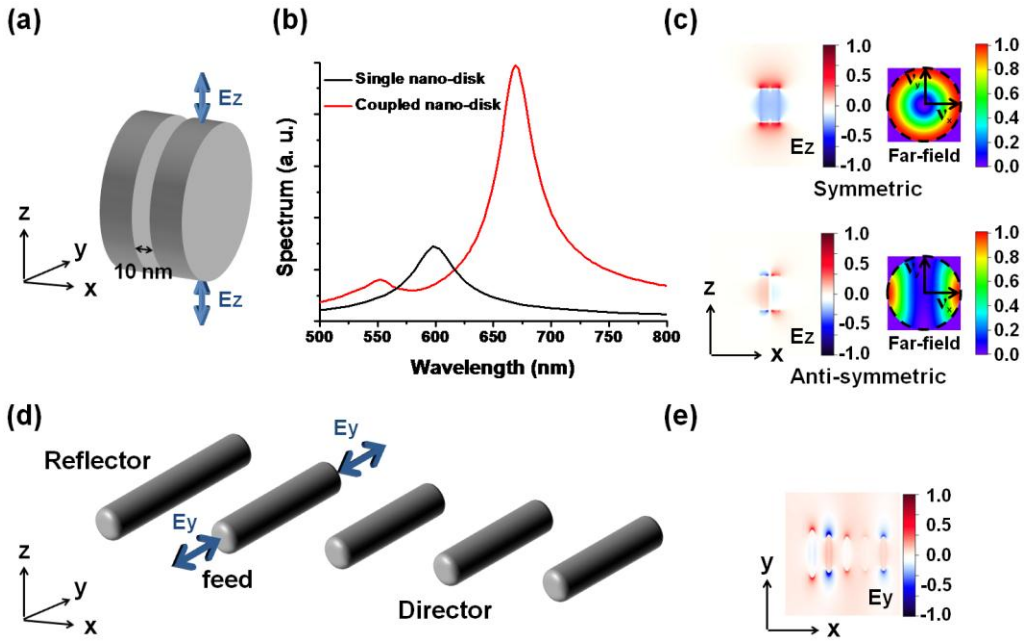

Fig. 3. (a) Schematic of coupled nano-disk structure. The diameter and the thickness of gold nano-disks are 90 nm and 20 nm, respectively. The surrounding media (including the middle gap between the two nano-disks) is the air ($\varepsilon = 1$). (b) Resonance spectrum of coupled nano-disk structure (red line) and a single nano-disk (black line). (c) Electric field profile and far-field radiation pattern of symmetric mode and anti-symmetric mode of coupled nano-disk structure. (d) Schematic of optical Yagi-Uda antenna in the air. The length of five elements are 200 nm (reflector), 160 nm (feed), and 144 nm (3 directors), respectively and the radius of the elements is 20 nm. Each elements have hemi-spherical ends. Reflector-feed distance is 130 nm and feed-director distance is 143 nm. (e) Electric field profile of optical Yagi-Uda antenna at resonance.

The coupled nano-disk structure consists of two identical gold disks [Fig. 3(a)]. A single nano-disk has a plasmon resonance at 600 nm as indicated by the black curve in Fig. 3(b), which shows the local field intensity spectrum when the structure is excited by dipole sources. If we place the two disks in the proximity such that the face-to-face distance is 10 nm, mode splitting occurs, having resonances at 551 nm and 665 nm [red curve in Fig. 3(b)]. If we follow the definition of mirror symmetry of vector field [14], the mode at 551 nm has an even parity with respect to the x-normal central symmetry plane and is called 'symmetric mode'. The other mode at 665 nm has an odd parity and is called 'anti-symmetric mode'. The electric field profile of the symmetric mode is similar to that of a z-directed electric dipole and the far-field radiation pattern of the symmetric mode resembles that of the z-directed electric dipole [Fig. 3(c)]. The anti-phase oscillations of the electric field of the anti-symmetric mode induces a virtual current loop around the y-axis, which results in the enhancement of the magnetic field in the y direction at the gap between the two disks. Therefore, the anti-symmetric mode behaves like a y-directed magnetic dipole and the far-field radiation pattern of the anti-symmetric mode is similar to that of the y-directed magnetic dipole as far as the propagation on the $z = 0$ plane ($\theta = \pi/2$) is concerned [Fig. 3(c)]. This mode splitting is also known as plasmon hybridization [15].

The coupled nano-disk structure is excited by placing monochromatic z-directed electric dipole oscillators 2 nm away from the edge of the front (+ x) disk [Fig. 3(a)]. By locating two dipole oscillators in an asymmetric fashion, both symmetric and anti-symmetric modes are excited simultaneously. We find that when the dipole is driven at a wavelength (670 nm), slightly detuned from the anti-symmetric resonance (665 nm), the symmetric and the anti-symmetric modes can be excited with the same amplitude and phase. In this case, the resultant

#148562 - $15.00 USD Received 1 Jun 2011; revised 23 Jun 2011; accepted 8 Jul 2011; published 19 Jul 2011

radiation [Fig. 4(a)] can be understood as that of a combination of the electric and the magnetic dipole oscillators as explained for the configuration of Fig. 2(c).

The second example, Yagi-Uda antenna consists of five cylindrical elements (1 feed, 1 reflector, 3 directors) which are made of aluminum. The designing rule of the antenna and the role of each element have been investigated theoretically [16] and experimentally [17]. The monochromatic y-directed electric dipoles oscillating at 600 nm are coupled to the feed element at the point of high electric field mode density, 2 nm outside from the apex of the feed [Fig. 3(d)]. The radiation becomes asymmetric [Fig. 4(b)] because the inductively detuned reflector reflects the emissions from the feed and the capacitively detuned directors guide the emissions to the front (+ x). This can be also explained by the similar way as in the case of the coupled nano-disk structure if we consider the electromagnetic field at the resonance to be the collection of y-directed electric dipoles and induced z-directed magnetic dipoles [Fig. 3(e)].

The spectral characteristics of the force conversion efficiency are summarized in Fig. 4. In order to investigate the spectral dependence we define a quantity, relative detuning (D).

$$D = \frac{\lambda - \lambda_{res}}{\lambda_{res}} \tag{9}$$

λ is wavelength and λ_{res} is the resonance wavelength of each structure.

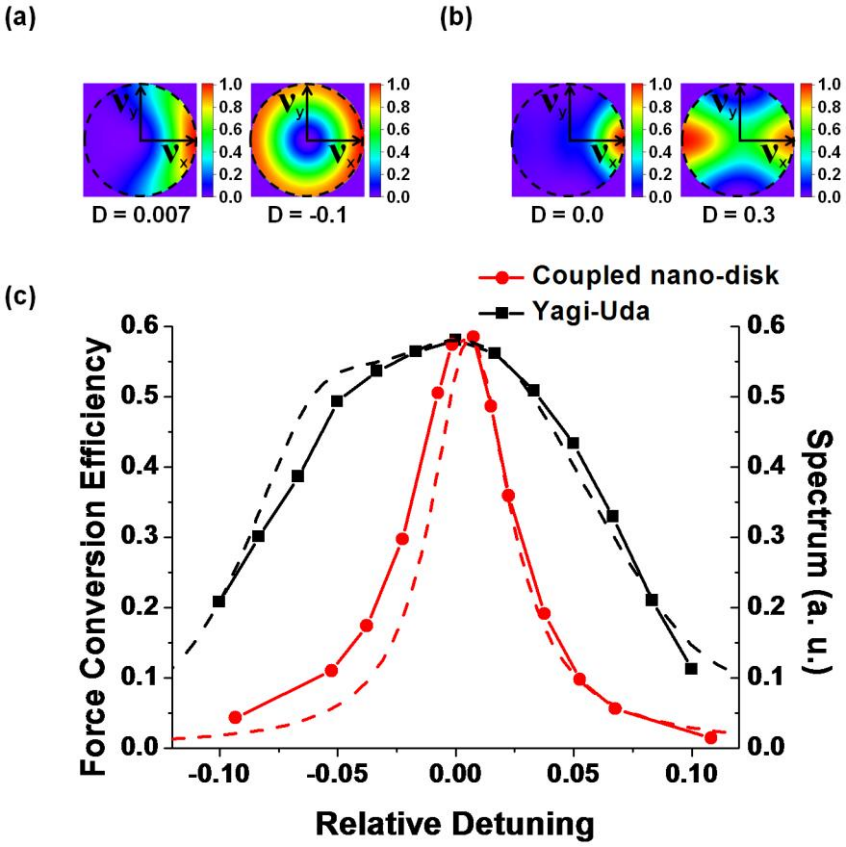

Fig. 4. (a) Far-field radiation pattern of coupled nano-disk structure. (b) Far-field radiation pattern of optical Yagi-Uda antenna. (c) Force conversion efficiency (lines with symbols) of coupled nano-disk structure and optical Yagi-Uda antenna. Also shown is the resonance spectra of coupled nano-disk (dashed-line in red) and optical Yagi-Uda antenna (dashed-line in black). $\lambda_{res} = \lambda_{anti\text{-}symmetric} = 665$ nm for coupled nano-disk structure. $\lambda_{res} = 600$ nm for optical Yagi-Uda antenna.

#148562 - $15.00 USD Received 1 Jun 2011; revised 23 Jun 2011; accepted 8 Jul 2011; published 19 Jul 2011

Firstly, the force conversion efficiency is large (~0.58 for both antenna) near the resonance wavelength (D ~0) as expected. Then, it decreases with the detuning. This is because the radiation is the most asymmetric near the resonance. For example, the radiation pattern of the coupled nano-disk structure at the small detuning (= 0.007) is highly asymmetric in the x direction [left panel of Fig. 4(a)]. However, when the detuning is sufficiently large, it becomes almost symmetric. At detuning of −0.1 (~2 FWHM), the radiation pattern of the coupled nano-disk structure looks similar to the toroidal radiation pattern of a point electric dipole oscillator. The optical Yagi-Uda antenna exhibits similar behavior [Fig. 4(b)].

Secondly, the spectral width of the force conversion efficiency follows that of the antenna resonance as shown in the Fig. 4(c). Since the full width half maximum (FWHM) of the spectrum is inversely proportional to the quality factor of the resonant mode (25 for the coupled nano-disk and 8.3 for optical Yagi-Uda antenna), the force conversion efficiency peak of the coupled nano-disk is one third sharper [FWHM of 0.05 in normalized wavelength (D) unit] than that of optical Yagi-Uda antenna (0.15).

5. Conclusion

In this work, it is shown that antennas with asymmetric radiation patterns can efficiently receive net recoil force upon light emission and that the force conversion efficiency is the maximum near the resonance wavelength. The equivalence of the far-field Poynting vector integration method to the Maxwell's stress tensor integration method for force calculation is explicitly proved. The directional nano-optical antenna can be utilized as a wavelength-selective optomechanical force generator where the generation of mechanical force is controlled by the wavelength of light source.

Acknowledgments

J. H. Song would like to thank Prof. Min-Kyo Seo at Korea Advanced Institute of Science and Technology for providing far-field calculation program. This work is supported by National Research Foundation Grants (2007-0093863, 2009-0087691, K20607000005, R31-2010-000-10071-0, 2009-351-C00115).

#148562 - $15.00 USD Received 1 Jun 2011; revised 23 Jun 2011; accepted 8 Jul 2011; published 19 Jul 2011